*Supporting Information*

# A highly conductive and antioxidative $MoO_2$-doped Li argyrodite electrolyte for all-solid-state Li batteries

Yinglei Wu,*[a] Runze Zhang,[ab] Qianjin Huang,[ab] Jingjing Wang,[b] Kaiyue Jiang,[bd] Zhenying Chen,[bc] Jinhui Zhu,*[b] Xiaodong Zhuang*[bd]

[a.] *School of Chemistry and Chemical Engineering, Shanghai University of Engineering Science, Shanghai 201620, China.*

[b.] *The Soft2D Lab, State Key Laboratory of Metal Matrix Composites, Shanghai Key Laboratory of Electrical Insulation and Thermal Ageing, School of Chemistry and Chemical Engineering, Shanghai Jiao Tong University, Shanghai 200240, China.*

*E-mail: zhujinhui1109@sjtu.edu.cn (J. Zhu), zhuang@sjtu.edu.cn (X. Zhuang)*

[c.] *College of Chemistry, Zhengzhou University, Zhengzhou 450001, Henan, China.*

[d.] *Frontiers Science Center for Transformative Molecules, Zhang Jiang Institute for Advanced Study, Shanghai Jiao Tong University, Shanghai 201203, China*

# 1. Experimental Procedures

## 1.1 Sulfide electrolytes synthesis

All preparations and sample treatments were carried out in an argon-filled glove box ($O_2$ and $H_2O$ < 0.01 ppm) owing to the extreme sensitivity of sulfide electrolytes to oxygen and moisture. The sulfide solid electrolytes (SSEs) were synthesized via conventional solid-state sintering. Analytical grade precursors, including lithium sulfide ($Li_2S$, Alfa, 99.98%), phosphorus pentasulfide ($P_2S_5$, Meryer, 99%), lithium chloride (LiCl, Sigma Aldrich, 99%), and $MoO_2$ (Aladdin, 99.9%) as raw materials were mixed with appropriate stoichiometric ratios according to $Li_{5.5+x}P_{1-x}Mo_xS_{4.5-2x}O_{2x}Cl_{1.5}$ (x = 0, 0.01, 0.02, 0.03) and then high-energy ball-milled at 550 rpm for 6 h. Subsequently, the obtained product was pressed into pellets and then sealed in quartz tubes for heat treatment. The tubes were heated up to 480 °C at the rate of 1 °C $min^{-1}$ and operated at 480 °C for 7 h. Until being completely cooled to ambient temperature, the obtained SSEs were ground for next-step use.

## 1.2 Characterization Methods

The morphology of as-prepared SSEs was measured by scanning electron microscope (SEM, EmCrafts CUBE II) equipped with energy dispersive spectroscopy (EDS). The crystal structure of as-prepared SSEs was analyzed by X-ray diffractometry (XRD, D8 ADVANCE Da Vinci, Cu Kα) in the range of 10 to 60°. The lattice parameters were refined by General Structure Analysis System (GSAS) software based on the Rietveld method. Raman spectra were recorded using K-Sens-532 under an incident laser beam at 532 nm. X-ray photoelectron spectroscopy (XPS) experiments were performed on an AXIS Ultra DLD system from Kratos, utilizing monochromatic Al Kα radiation (1486.6 eV) with a C 1s value set at 284.8 eV for charge corrections. One-pulse $^7Li$ magic angle spinning nuclear magnetic resonance (MAS NMR) spectra were acquired with an AVANCE NEO 600.13 MHz.

### 1.3 Electrochemical measurements

The ionic conductivities of as-prepared $Li_{5.5+x}P_{1-x}Mo_xS_{4.5-2x}O_{2x}Cl_{1.5}$ (x = 0, 0.01, 0.02, 0.03) SSEs were determined by electrochemical impedance spectroscopy (EIS) from 25 to 65 °C using the electrochemical station (EC-Lab SP-300) in the frequency range from 0.1 Hz to 7.0 MHz under 10 mV driving amplitude. Prior to the measurements, electrolyte powders (120 mg) were pressed into pellets (diameter: 10 mm, thickness: ~ 1 mm) under a pressure of ~ 350 MPa, and then indium (In) foils as the current collectors were placed and pressed on the pellet surfaces in a model cell. The electronic conductivities were measured by the direct current (DC) polarization method in a stainless-steel symmetric cell under different voltages. The linear sweep voltammetry (LSV) curves of the Li-In|SSEs|(SSEs+carbon) cells were tested at a scanning rate of 5 mV $s^{-1}$ in the range of 2 to 6 V vs. $Li/Li^+$.

### 1.4 Full cell assembly and tests

The composite cathode powder was synthesized by dry ball milling a blend of single-crystal $LiNi_{0.8}Co_{0.1}Mn_{0.1}O_2$ (NCM811, Canrd Technology Co., Ltd., 70 wt%), as-prepared SSEs (29 wt%), and vapor-grown carbon fiber (VGCF, Canrd Technology Co., Ltd., 1 wt%) at 360 rpm for 4 h under an Ar atmosphere.

All full cell assembly procedures were conducted within an Ar-filled glovebox, ensuring low levels of oxygen ($O_2$ < 0.1 ppm) and moisture ($H_2O$ < 0.1 ppm). The full cells were assembled using specialized cell molds comprised of two conductive die steel bars and a poly(ether ether-ketone) cylinder with an internal diameter of 1 cm. The process began by pressing 90 mg of as-prepared SSEs at 80 MPa for 30 s to form a pellet with a diameter of 1 cm. Next, a composite cathode powder with NCM811 loading of 5.6 mg $cm^{-2}$ was evenly spread on one side of the pellet, followed by further pressing at 360 MPa for 30 s to create a two-layer pellet. Finally, the Li-In anode was placed on the other side of the SSE pellet to form a sandwich structure, which was then inserted into the cell mold.

Before commencing cell tests, the assembled cell mold underwent stack pressure (35

MPa) via a digital tablet press, maintaining the operating pressure by securing the cell between two steel plates with bolts at each corner. All cycling procedures for the full cells were conducted using a Neware Battery cycler at room temperature (RT). The galvanostatic charge–discharge cycling tests were carried out within a voltage range of 2.5–3.7 V. The rate capability test of the cell involved rates of 0.1, 0.2, 0.5, 1, 2, and 3 C (1 C = 200 mA $g^{-1}$), respectively, for 5 cycles at each density. For long cycling stability testing, the initial two cycles ran at a rate of 0.1 C, followed by subsequent cycles at 1 C. For the GITT measurement. All the cells were first charged at a constant current of C/10 to the voltage reached 3.7 V and then discharged for 10 min at a constant current of C/10 and rested for 60 min until the voltage reached 2.5 V. EIS tests of the full cells were conducted using a Bio-Logic SP300 potentiostat, covering a frequency range from 100 kHz to 0.1 Hz with an amplitude of 10 mV.

### 1.5 Moisture stability tests

The $H_2S$ gas concentration generated from a 100 mg cold-pressed pellet was monitored via a sensor (BH-90A, Baoshian Electronic Technology Co., Ltd).

## 2. Supplementary Figures

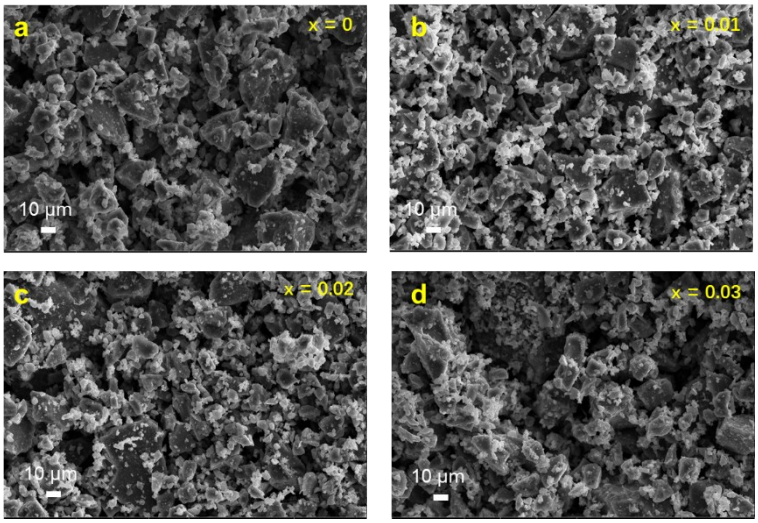


**Fig. S1** SEM images of $Li_{5.5+x}P_{1-x}Mo_xS_{4.5-2x}O_{2x}Cl_{1.5}$ (x = 0, 0.01, 0.02, 0.03) SSEs.

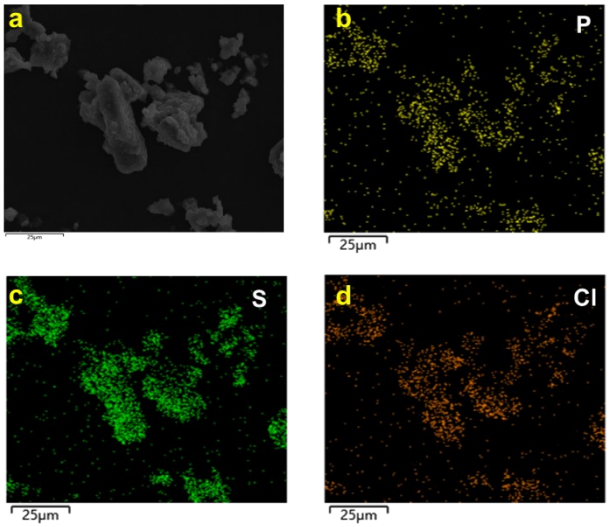


**Fig. S2** Elemental distribution of $Li_{5.5}PS_{4.5}Cl_{1.5}$ SSE

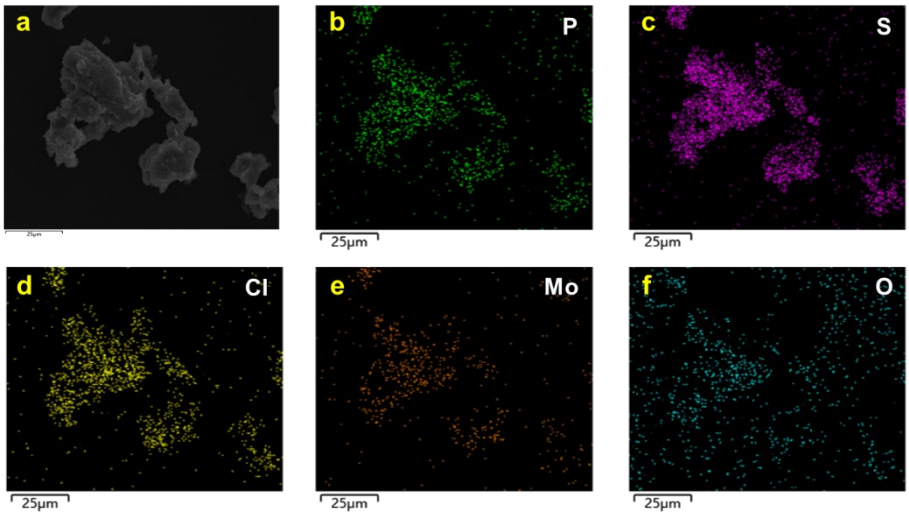


**Fig. S3** Elemental distribution of $Li_{5.5+x}P_{1-x}Mo_xS_{4.5-2x}O_{2x}Cl_{1.5}$ (x = 0.01) SSE.

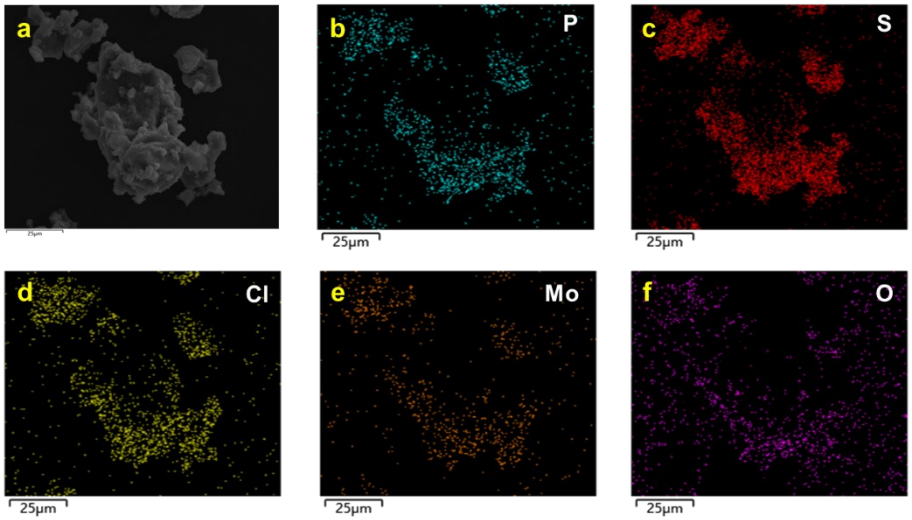


**Fig. S4** Elemental distribution of $Li_{5.5+x}P_{1-x}Mo_xS_{4.5-2x}O_{2x}Cl_{1.5}$ (x = 0.02) SSE.

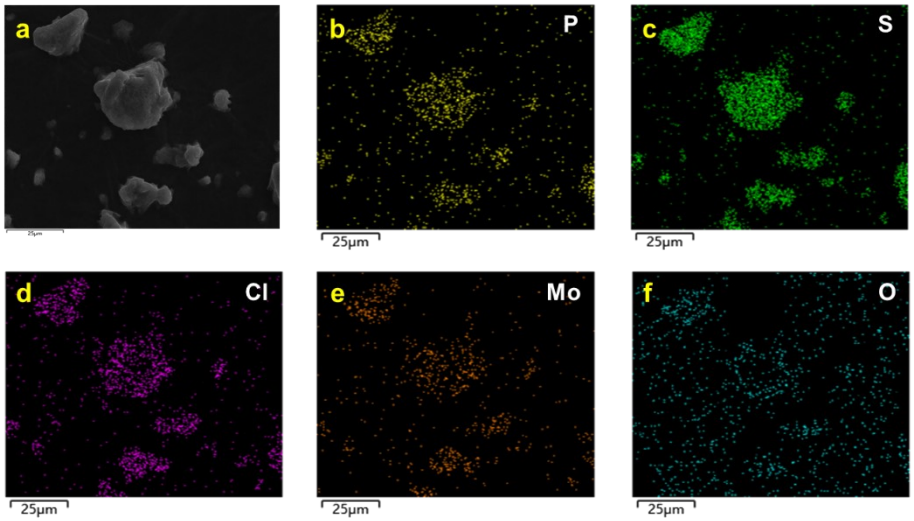


**Fig. S5** Elemental distribution of $Li_{5.5+x}P_{1-x}Mo_xS_{4.5-2x}O_{2x}Cl_{1.5}$ (x = 0.03) SSE.

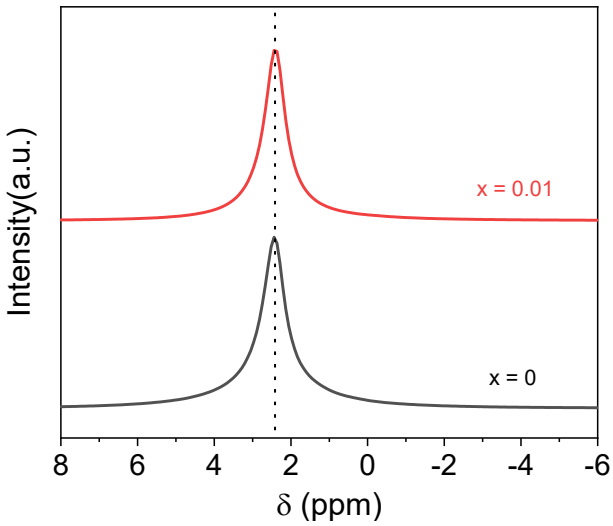


**Fig. S6** 7Li MAS NMR spectra of $Li_{5.51}P_{0.99}Mo_{0.01}S_{4.48}O_{0.02}Cl_{1.5}$ and $Li_{5.5}PS_{4.5}Cl_{1.5}$ electrolytes.

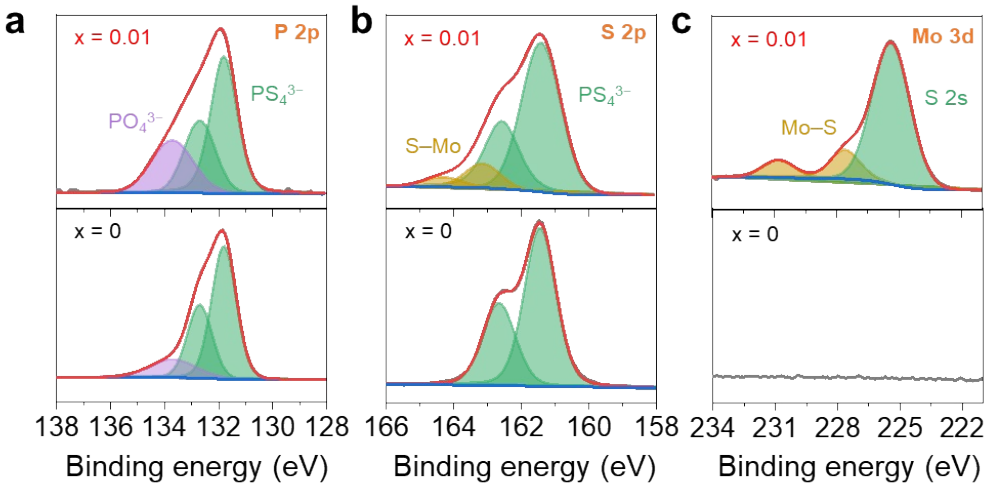


**Fig. S7** P 2p (a), S 2p (b), and Mo 3d (c) XPS spectra of $Li_{5.51}P_{0.99}Mo_{0.01}S_{4.48}O_{0.02}Cl_{1.5}$ and $Li_{5.5}PS_{4.5}Cl_{1.5}$ electrolytes.

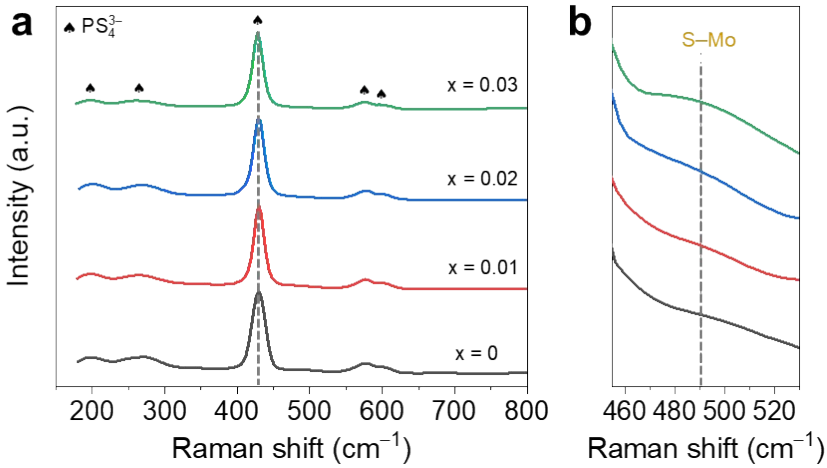


**Fig. S8** Raman spectra of $Li_{5.5+x}P_{1-x}Mo_xS_{4.5-2x}O_{2x}Cl_{1.5}$ (x = 0, 0.01, 0.02, 0.03) electrolytes.

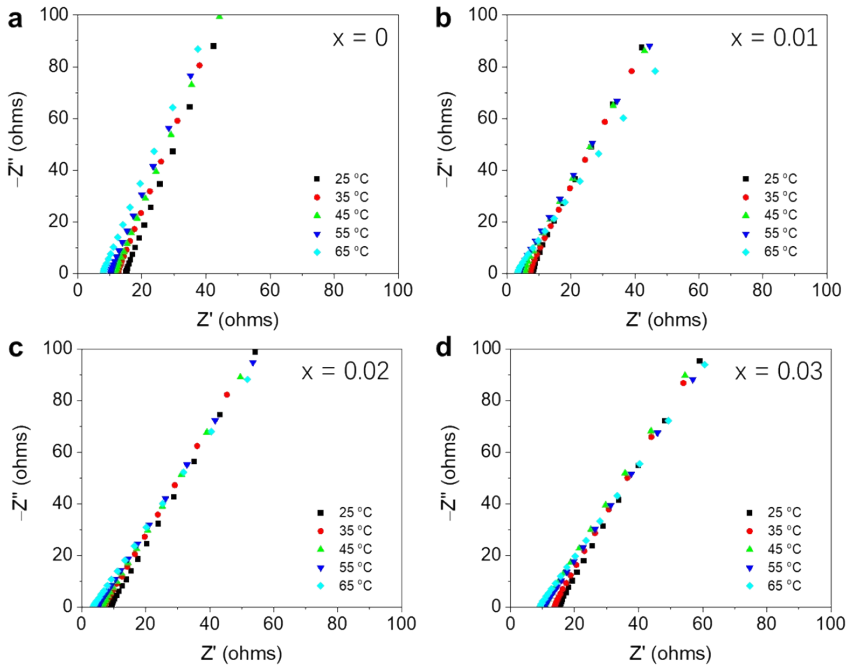


**Fig. S9** Nyquist plots of $Li_{5.5+x}P_{1-x}Mo_xS_{4.5-2x}O_{2x}Cl_{1.5}$ (x = 0, 0.01, 0.02, 0.03) electrolytes as a function of with temperature from 25 to 65 °C.

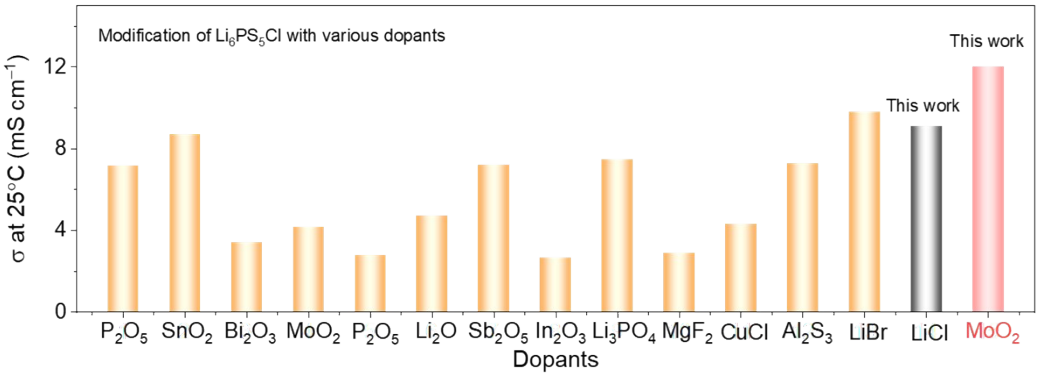


**Fig. S10** Ionic conductivity comparison of modified $Li_6PS_5Cl$ electrolytes with various dopants.

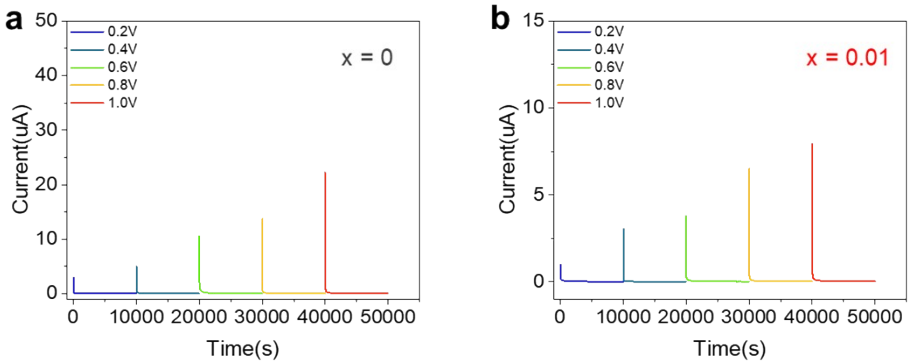


**Fig. S11** Chronoamperometric measurements of $Li_{5.5}PS_{4.5}Cl_{1.5}$ (a) and $Li_{5.51}P_{0.99}Mo_{0.01}S_{4.48}O_{0.02}Cl_{1.5}$ (b) electrolytes at different voltages.

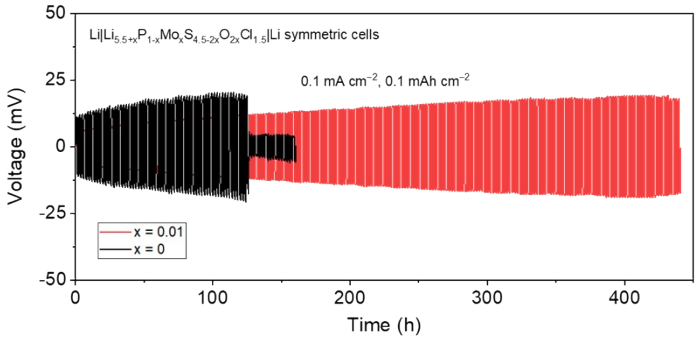


**Fig. S12** Cycle stability of Li|Li symmetric cells with as-prepared SSEs.

We assembled and evaluated Li|SSE|Li symmetric cells under 0.1 mA $cm^{-2}$ and 0.1 mAh $cm^{-2}$, as shown in Fig. S12. The Li|Li cell with 1 wt% $MoO_2$-doped SSE demonstrated stability for nearly 450 h of cycling, with the overpotential increasing only from approximately 7 to 19 mV. In contrast, the Li|Li cell with undoped SSE sustained operation for just 120 h, showing a large overpotential of 11–19 mV, which ultimately led to sudden short-circuiting. These results indicate that $MoO_2$-doped SSE forms a more stable interface with Li/Li-alloy anodes.

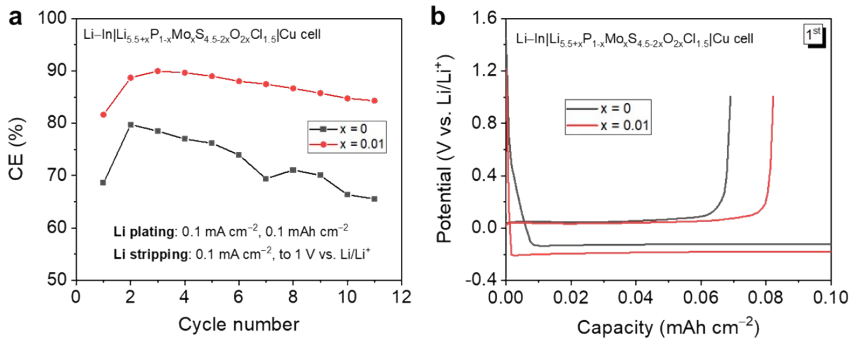


**Fig. S13** Li plating/stripping CE (a) and 1st voltage profiles (b) of Li|Cu cells with prepared SSEs.

To evaluate the CE of Li plating and stripping with $MoO_2$-doped SSE, we assembled and tested Li|Cu cells with the prepared SSEs. As shown in Fig. S13a, the Li|Cu cell using 1% $MoO_2$-doped SSE exhibits an initial CE of 81.6% and an average CE of 86.9% over 11 cycles, both of which surpass the values of the cell with undoped SSE (68.6% and 72.4%). Additionally, the $MoO_2$-doped cell shows more stable cycling. From the voltage profiles of the Li|Cu cells (Fig. S13b), the $MoO_2$-doped SSE demonstrates negligible side reactions with Li metal, while the undoped SSE experiences severe side reactions.

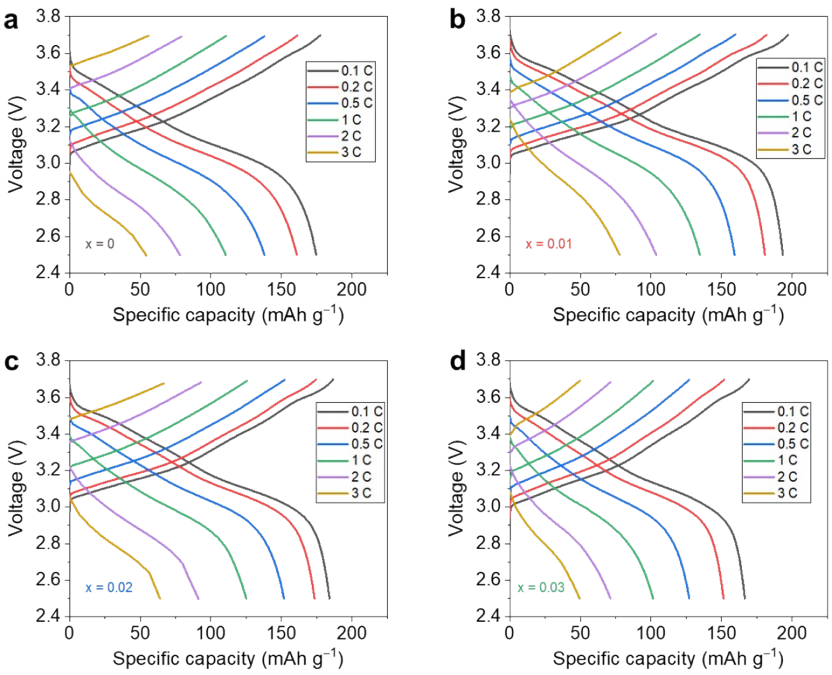


**Fig. S14** Voltage profiles of full cells with $Li_{5.5+x}P_{1-x}Mo_xS_{4.5-2x}O_{2x}Cl_{1.5}$ (x = 0, 0.01, 0.02, 0.03) electrolytes at various rates.

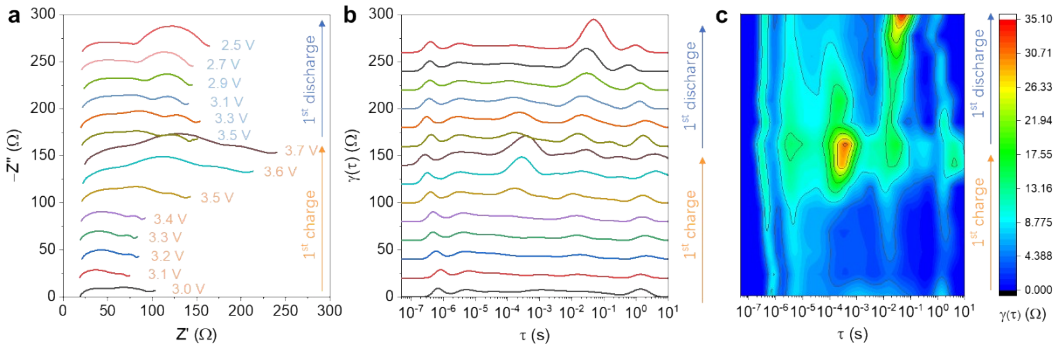


**Fig. S15** In situ Nyquist plots (a), calculated DRT spectra (b), and corresponding 2D intensity color map (c) of the cell with $Li_{5.51}P_{0.99}Mo_{0.01}S_{4.48}O_{0.02}Cl_{1.5}$ electrolyte.

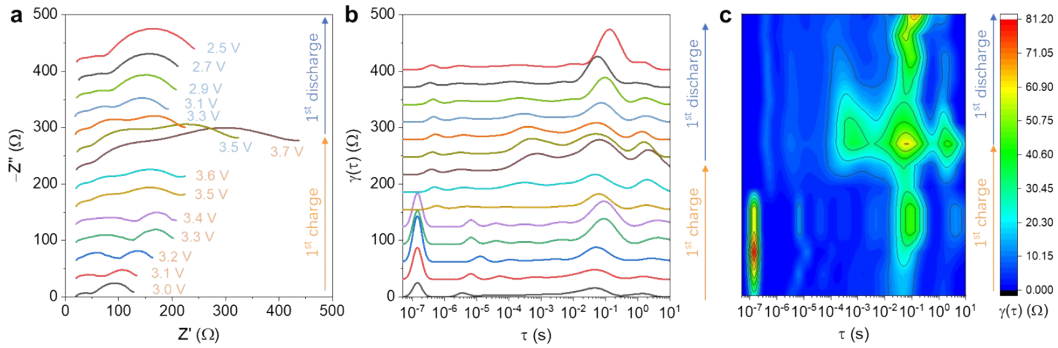


**Fig. S16** In situ Nyquist plots (a), calculated DRT spectra (b), and corresponding 2D intensity color map (c) of the cell with $Li_{5.5}PS_{4.5}Cl_{1.5}$ electrolyte.

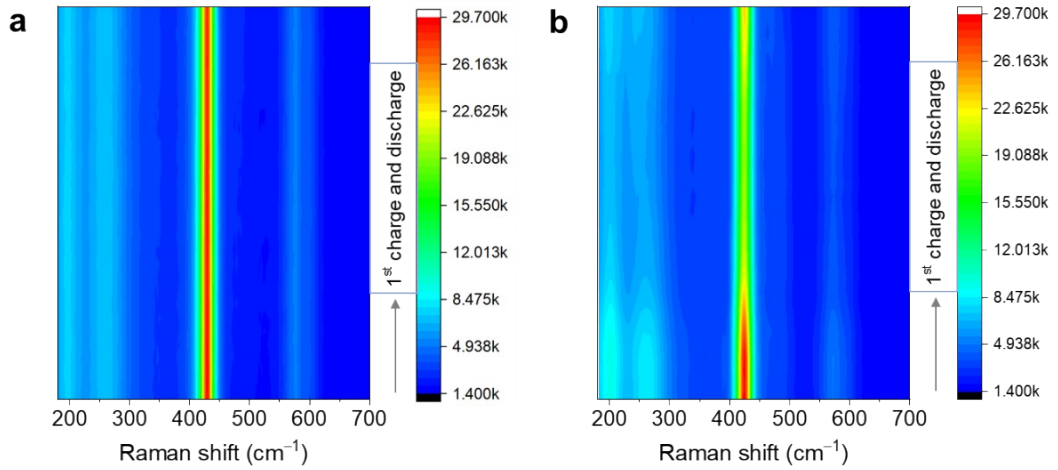


**Fig. S17** In situ Raman spectra collected at cathodic interface with (a) $Li_{5.51}P_{0.99}Mo_{0.01}S_{4.48}O_{0.02}Cl_{1.5}$, and (b) $Li_{5.5}PS_{4.5}Cl_{1.5}$ electrolytes.

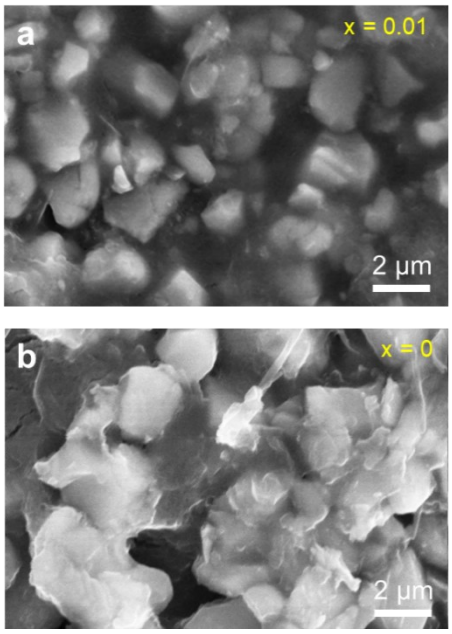


**Fig. S18** SEM images of cycled composite cathodes with (a) $Li_{5.51}P_{0.99}Mo_{0.01}S_{4.48}O_{0.02}Cl_{1.5}$, and (b) $Li_{5.5}PS_{4.5}Cl_{1.5}$ electrolytes.

# 3. Supplementary Tables

**Table S1** Crystallographic data of $Li_{5.51}P_{0.99}Mo_{0.01}S_{4.48}O_{0.02}Cl_{1.5}$ (space group = *F-43m*) obtained from Rietveld refinement of X-ray diffraction data.

| **Atom** | **Wyckoff site** | ***x*** | ***y*** | ***z*** | **Occ.** | **U (Å$^2$)** |
|---|---|---|---|---|---|---|
| **Li** | 48*h* | 0.3263 | 0.0173 | 0.6728 | 0.5 | 0.175 |
| **P** | 4*b* | 0 | 0 | 0.5 | 0.989 | 0.022 |
| **Mo** | 4*b* | 0 | 0 | 0.5 | 0.011 | 0.022 |
| **S1** | 16*e* | 0.1176 | -0.1176 | 0.6176 | 0.948 | 0.020 |
| **O** | 16*e* | 0.1176 | -0.1176 | 0.6176 | 0.052 | 0.020 |
| **S2** | 4*a* | 0 | 0 | 1 | 0.385 | 0.028 |
| **S3** | 4*d* | 0.25 | 0.25 | 0.75 | 0.166 | 0.031 |
| **Cl1** | 4*a* | 0 | 0 | 1 | 0.615 | 0.028 |
| **Cl2** | 4*d* | 0.25 | 0.25 | 0.75 | 0.834 | 0.031 |

**Table S2** Summary of electrochemical properties of as-prepared SSEs compared with other representative SSEs.

| Solid electrolyte composition | Dopant/ Substitute | Ionic conductivity (mS $cm^{-1}$) | Activation energy (eV) | Electron conductivity (S $cm^{-1}$) | Ref. |
|---|---|---|---|---|---|
| $Li_{5.5}PS_{4.425}O_{0.075}Cl_{1.5}$ | $P_2O_5$ | 7.15 | NA | NA | 1 |
| $Li_{5.5}P_{0.9}Sn_{0.1}S_{4.2}O_{0.2}Cl_{1.6}$ | $SnO_2$ | 8.7 | 0.18 | NA | 2 |
| $Li_{6.04}P_{0.98}Bi_{0.02}S_{4.97}O_{0.03}Cl$ | $Bi_2O_3$ | 3.4 | 0.261 | $5.3\times10^{-9}$ | 3 |
| $Li_6PS_{4.7}O_{0.3}Br$ | $Li_2O$ | 1.54 | NA | NA | 4 |
| $Li_6PS_5Cl$-$MoO_2$-0.05 | $MoO_2$ | 4.16 | 0.299 | $2.04\times10^{-8}$ | 5 |
| $Li_{5.7}Zn_{0.15}PS_{4.85}O_{0.15}Br$ | ZnO | 1.59 | NA | $8\times10^{-11}$ | 6 |
| LPSI-$SnO_2$-0.3 | $SnO_2$ | 0.234 | 0.32 | NA | 7 |
| $Li_{6.25}PS_4O_{1.25}Cl_{0.75}$ | $Li_2O$, $P_2O_5$ | 2.8 | 0.33 | $1.91\times10^{-8}$ | 8 |
| $Li_6PS_{4.75}ClO_{0.25}$ | $Li_2O$ | 4.7 | 0.288 | NA | 9 |
| $Li_{5.5}P_{0.96}Sb_{0.04}S_{4.40}O_{0.10}Cl_{1.5}$ | $Sb_2O_5$ | 7.2 | 0.27 | $4\times10^{-9}$ | 10 |
| $Li_{5.65}[Si_{0.05}Ge_{0.05}Sn_{0.05}P_{0.85}][S_{4.5}Cl_{0.5}]Br$ | $SiS_2$, $GeS_2$, $SnS_2$ | 7.96 | 0.18 | NA | 11 |
| $Li_{6.16}P_{0.92}In_{0.08}S_{4.88}O_{0.12}Cl$ | $In_2O_3$ | 2.67 | 0.278 | $1.87\times10^{-9}$ | 12 |
| $Li_{6.3}P_{0.9}Mg_{0.1}S_5Cl_{0.8}F_{0.2}$ | $MgF_2$ | 2.91 | 0.32 | $1.03\times10^{-9}$ | 13 |
| $Li_{6.3}P_{0.9}Cu_{0.1}S_{4.9}Cl_{1.1}$ | CuCl | 4.34 | 0.25 | $1.49\times10^{-9}$ | 14 |
| $Li_{6.5}In_{0.25}P_{0.75}S_5I$ | In | 1.06 | 0.276 | $8.32\times10^{-9}$ | 15 |
| $Li_{5.4}Al_{0.1}PS_{4.7}Cl_{1.3}$ | $Al_2S_3$ | 7.29 | 0.16 | NA | 16 |
| $Li_{5.5}PS_{4.5}Cl_{0.8}Br_{0.7}$ | LiBr | 9.6 | 0.30 | NA | 17 |
| $Li_{5.51}P_{0.99}Mo_{0.01}S_{4.48}O_{0.02}Cl_{1.5}$ | $MoO_2$ | 12.0 | 0.28 | $1.73\times10^{-9}$ | This work |

**Table S3** Summary of the electrochemical performance of SSEs-based ASSLBs.

| SSE | Cathode | Anode | Rate | Capacity ($mAh\ g^{-1}$) | Stability | Ref. |
|---|---|---|---|---|---|---|
| $Li_{5.5}PS_{4.425}O_{0.075}Cl_{1.5}$ | NCM811 | Li-In | 0.2 C | 160.2 | 100/95.1% | 1 |
| $Li_{5.5}P_{0.9}Sn_{0.1}S_{4.2}O_{0.2}Cl_{1.6}$ | NCM811 | Li-In | 0.5 C | 119.1 | 100/74.7% | 2 |
| $Li_6PS_{4.7}O_{0.3}Br$ | NCM811 | Li-In | 0.1 C | 108.7 | NA | 4 |
| $Li_6PS_{4.75}ClO_{0.25}$ | $LiCoO_2$ | Li-In | 0.3 C | 89 | 250/86% | 9 |
| $Li_{5.5}P_{0.96}Sb_{0.04}S_{4.40}O_{0.10}Cl_{1.5}$ | NCM622 | Li-In | 0.1 C | 162.4 | 80/99% | 10 |
| $Li_{5.65}[Si_{0.05}Ge_{0.05}Sn_{0.05}P_{0.85}][S_{4.5}Cl_{0.5}]Br$ | NCM712 | Li-In | 5 C | 96 | 1400/85.6% | 11 |
| $Li_{5.5}PS_{4.5}Cl_{0.8}Br_{0.7}$ | NCM90 | Li-In | 2 C | 108 | 700/123% | 17 |
| $Li_6PS_5Cl$ | NCM811 | Li-In | 0.1 C | 180 | 50/97% | 18 |
| $Li_{5.5}PS_{4.5}Cl_{1.5}$ | NCM85 | Li-In | 0.5 C | 170 | 50/85% | 19 |
| $Li_{5.51}P_{0.99}Mo_{0.01}S_{4.48}O_{0.02}Cl_{1.5}$ | NCM811 | Li-In | 0.1 C | 194 | 3500/80% | This work |

**Table S4** Equivalent circuit fitting of in situ EIS spectra of full cells with as-prepared SSEs.

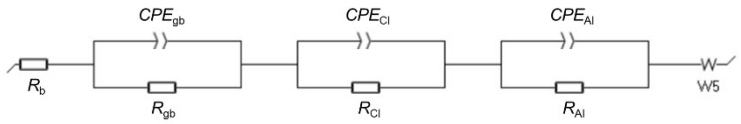


| | Voltage | $R_b$ | | $R_{gb}$ | | $R_{CI}$ | | $R_{AI}$ | |
|---|---|---|---|---|---|---|---|---|---|
| | (V) | Cell-1 | Cell-0 | Cell-1 | Cell-0 | Cell-1 | Cell-0 | Cell-1 | Cell-0 |
| **Charge** | **3.0** | 17.58 | 19.37 | 12.27 | 20.25 | 20.80 | 70.37 | 21.23 | 25.62 |
| | **3.1** | 17.30 | 20.64 | 13.11 | 21.62 | 21.36 | 86.53 | 22.43 | 26.22 |
| | **3.2** | 19.38 | 19.24 | 13.68 | 20.04 | 21.89 | 98.15 | 23.73 | 25.06 |
| | **3.3** | 19.08 | 17.77 | 14.21 | 21.22 | 24.72 | 129.13 | 24.03 | 35.72 |
| | **3.4** | 20.19 | 21.25 | 14.08 | 19.40 | 27.76 | 179.98 | 27.75 | 56.03 |
| | **3.5** | 19.81 | 19.22 | 14.73 | 22.40 | 41.66 | 204.70 | 62.03 | 62.10 |
| | **3.6** | 19.33 | 20.21 | 12.89 | 23.55 | 56.25 | 262.10 | 101.71 | 74.82 |
| | **3.7** | 23.18 | 20.26 | 12.20 | 22.30 | 63.80 | 321.13 | 151.66 | 126.12 |
| **Discharge** | **3.5** | 17.29 | 21.69 | 11.30 | 14.40 | 62.52 | 219.47 | 55.52 | 86.00 |
| | **3.3** | 19.45 | 18.95 | 13.70 | 14.77 | 65.57 | 104.55 | 45.62 | 72.10 |
| | **3.1** | 17.69 | 18.35 | 10.11 | 16.02 | 79.45 | 103.40 | 27.95 | 60.87 |
| | **2.9** | 18.69 | 20.98 | 11.86 | 19.47 | 86.13 | 140.65 | 24.80 | 32.70 |
| | **2.7** | 17.30 | 21.39 | 12.75 | 22.00 | 95.42 | 153.91 | 19.49 | 24.87 |
| | **2.5** | 20.58 | 18.85 | 12.36 | 19.09 | 108.69 | 239.80 | 18.78 | 30.04 |

Note:

$R_b$: impedance of bulk electrolyte;

$R_{gb}$: impedance of grain boundary of electrolyte;

$R_{CI}$: impedance of cathodic interface;

$R_{AI}$: impedance of anodic interface;

Cell-1: Li-In|NCM811 full cell with $Li_{5.51}P_{0.99}Mo_{0.01}S_{4.48}O_{0.02}Cl_{1.5}$ electrolyte;

Cell-0: Li-In|NCM811 full cell with $Li_{5.5}PS_{4.5}Cl_{1.5}$ electrolyte.

**Table S5** The percentage of P and S species in cycled and fresh composite cathodes.

| | P elements | | | S elements | | | |
|---|---|---|---|---|---|---|---|
| | $PS_4^{3-}$ | $PO_4^{3-}$ | $P_2O_5$ | $PS_4^{3-}$ | S–Mo | S–S | Sulfate |
| Cycled composite cathode with $Li_{5.51}P_{0.99}Mo_{0.01}S_{4.48}O_{0.02}Cl_{1.5}$ | 73.26% | 26.74% | -- | 76.62 | 17.94% | -- | 5.44% |
| Fresh $Li_{5.51}P_{0.99}Mo_{0.01}S_{4.48}O_{0.02}Cl_{1.5}$ | 73.09% | 26.91% | -- | 88.03% | 11.97% | -- | -- |
| Cycled composite cathode with $Li_{5.5}PS_{4.5}Cl_{1.5}$ | 63.93% | 19.95% | 16.12% | 61.34% | -- | 20.73% | 17.93% |
| Fresh $Li_{5.5}PS_{4.5}Cl_{1.5}$ | 85.93% | 14.07% | -- | 100% | -- | -- | -- |

# 4 References


1. L. Peng, S. Chen, C. Yu, C. Wei, C. Liao, Z. Wu, H. L. Wang, S. Cheng and J. Xie, *ACS Appl. Mater. Interfaces*, 2022, **14**, 4179-4185.
2. G. Li, S. Wu, H. Zheng, Y. Yang, J. Cai, H. Zhu, X. Huang, H. Liu and H. Duan, *Adv. Funct. Mater.*, 2022, **32**, 2211805.
3. H. Liu, Q. Zhu, C. Wang, G. Wang, Y. Liang, D. Li, L. Gao and L. Z. Fan, *Adv. Funct. Mater.*, 2022, **32**, 2203858.
4. Z. Zhang, L. Zhang, X. Yan, H. Wang, Y. Liu, C. Yu, X. Cao, L. van Eijck and B. Wen, *J. Power Sources*, 2019, **410-411**, 162-170.
5. Y. Subramanian, R. Rajagopal, S. Kang and K.-S. Ryu, *J. Alloys Compd.*, 2022, **925**, 166596.
6. T. Chen, L. Zhang, Z. Zhang, P. Li, H. Wang, C. Yu, X. Yan, L. Wang and B. Xu, *ACS Appl. Mater. Interfaces*, 2019, **11**, 40808-40816.
7. T. Chen, D. Zeng, L. Zhang, M. Yang, D. Song, X. Yan and C. Yu, *J. Energy Chem.*, 2021, **59**, 530-537.
8. H. Xu, G. Cao, Y. Shen, Y. Yu, J. Hu, Z. Wang and G. Shao, *Energy Environ. Mater.*, 2022, **5**, 852-864.
9. Z. Sun, Y. Lai, N. Lv, Y. Hu, B. Li, L. Jiang, J. Wang, S. Yin, K. Li and F. Liu, *ACS Appl. Mater. Interfaces*, 2021, **13**, 54924-54935.
10. C. Wei, C. Yu, R. Wang, L. Peng, S. Chen, X. Miao, S. Cheng and J. Xie, *J. Power Sources*, 2023, **559**, 232659.
11. W. Li, Z. Chen, Y. Chen, L. Zhang, G. Liu and L. Yao, *Adv. Funct. Mater.*, 2024, **34**, 2312812.
12. C. Wang, J. Hao, J. Wu, H. Shi, L. Fan, J. Wang, Z. Wang, Z. Wang, L. Yang, Y. Gao, X. Yan and Y. Gu, *Adv. Funct. Mater.*, 2024, **34**, 2313308.
13. C. Liu, B. Chen, T. Zhang, J. Zhang, R. Wang, J. Zheng, Q. Mao and X. Liu, *Angew. Chem. Int. Ed.*, 2023, **62**, e202302655.
14. B. W. Taklu, W.-N. Su, Y. Nikodimos, K. Lakshmanan, N. T. Temesgen, P.-X. Lin, S.-K. Jiang, C.-J. Huang, D.-Y. Wang, H.-S. Sheu, S.-H. Wu and B. J. Hwang, *Nano Energy*, 2021, **90**, 106542.
15. Z. Jiang, H. Peng, Y. Liu, Z. Li, Y. Zhong, X. Wang, X. Xia, C. Gu and J. Tu, *Adv. Energy Mater.*, 2021, **11**, 2101521.
16. Y. J. Choi, S. I. Kim, M. Son, J. W. Lee and D. H. Lee, *Nanomaterials*, 2022, **12**, 4355.
17. S. Li, J. Lin, M. Schaller, S. Indris, X. Zhang, T. Brezesinski, C. W. Nan, S. Wang and F. Strauss, *Angew. Chem. Int. Ed.*, 2023, **62**, e202314155.
18. E. Schlautmann, A. Weiß, O. Maus, L. Ketter, M. Rana, S. Puls, V. Nickel, C. Gabbey, C. Hartnig, A. Bielefeld and W. G. Zeier, *Adv. Energy Mater.*, 2023, **13**, 2302309.
19. T. T. Zuo, F. Walther, J. H. Teo, R. Ruess, Y. Wang, M. Rohnke, D. Schroder, L. F. Nazar and J. Janek, *Angew. Chem. Int. Ed.*, 2023, **62**, e202213228.